Cellulose (2020) 27:3517–3530
https://doi.org/10.1007/s10570-020-03007-x

ORIGINAL RESEARCH

A facile method for fabricating color adjustable multifunctional cotton fabrics with solid solution $BiOBr_xI_{1-x}$ nanosheets

Peiwen Zhou · Linping Zhang · Xiaofeng Sui · Yi Zhong · Bijia Wang · Zhize Chen · Xueling Feng · Hong Xu · Zhiping Mao

Received: 29 August 2019 / Accepted: 18 January 2020 / Published online: 29 January 2020

Abstract Multifunctional cotton fabric with adjustable color was simply fabricated by anchoring solid solution $BiOBr_xI_{1-x}$ nanosheets on the surface of carboxymethylated cotton fabric for self-cleaning, UV protection, and near infrared reflection. The structure and morphology of prepared multifunctional cotton fabrics ($BiOBr_xI_{1-x}$-CCF ($0 \leq x \leq 1$)) were characterized by X-ray powder diffraction and scanning electron microscopy. Color, self-cleaning, UV protection, near infrared reflection, and acid and alkali resistance of these multifunctional cotton fabrics were systematically studied. With the increase of iodine content, the $BiOBr_xI_{1-x}$ nanosheets with an average thickness of 40–50 nm and a size of 1–2 μm in the other two dimensions loaded on the cotton fabrics can extend the absorption edge of $BiOBr_xI_{1-x}$-CCF ($0 \leq x \leq 1$) from 430 nm to 630 nm, giving cotton fabric color and excellent UV protection property. Interlaced solid solution nanosheets on cotton fabric surface give $BiOBr_xI_{1-x}$-CCF hydrophobicity (contact angle: 139°–143°) and ability to photodegrade stain under the visible light irradiation. The near infrared reflectance of $BiOBr_xI_{1-x}$-CCF ($0 \leq x \leq 1$) is higher than that of the raw cotton, which gives it infrared reflection thermal isolation. $BiOBr_xI_{1-x}$-CCF ($0 \leq x \leq 1$) has a certain acid and alkali resistance in solution (pH 2.3–11.2). Thus, $BiOBr_xI_{1-x}$-CCF has great potential to be used as multifunctional fabric in self-cleaning and outdoor protection.

Electronic supplementary material The online version of this article (https://doi.org/10.1007/s10570-020-03007-x) contains supplementary material, which is available to authorized users.

P. Zhou · L. Zhang · X. Sui · Y. Zhong · B. Wang · Z. Chen · X. Feng · H. Xu (✉) · Z. Mao (✉)
Key Lab of Science and Technology of Eco-textile, Ministry of Education, College of Chemistry, Chemical Engineering and Biotechnology, Innovation Center for Textile Science and Technology, Donghua University, No. 2999 North Renmin Road, Shanghai 201620, China
e-mail: hxu@dhu.edu.cn

Z. Mao
e-mail: zhpmao@dhu.edu.cn

H. Xu · Z. Mao
Collaborative Innovation Center for Eco-Textiles of Shandong Province, Qingdao University, Qingdao 266071, China

Graphic abstract

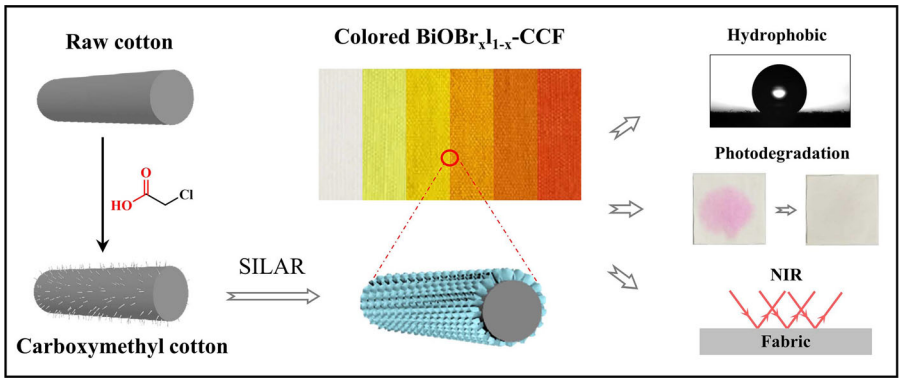

Keywords $BiOBr_xI_{1-x}$ solid solution · Adjustable color · Self-cleaning · UV protection · Near infrared reflection · Cotton fabric

Introduction

Cotton is an abundant renewable natural cellulose material. It has many advantages (Hu et al. 2018) such as hydrophilicity, softness, reproducibility, processability, and biodegradability, which make it widely used as a wearable material. With the development of industrialization and the emphasis on environmental protection, renewable and easily biodegradable cellulosic materials have more uses in industrial textile materials (Chen et al. 2018a), such as wall cloth, awning, tents, table cloth, and curtains. These applications require cotton fabric with some special features such as adjustable color, self-cleaning, UV absorption and near infrared reflection properties.

In the last 10 years, photocatalysts as the new materials, especially for TiO_2 and ZnO (Chen et al. 2018a; Hu et al. 2018; Ma et al. 2019), are widely used in fabricating multifunctional cotton fabric due to ultraviolet absorption, photodegrading contaminants, superhydrophobicity, and near infrared reflection property (Ge et al. 2018; Ge et al. 2020; Moridi Mahdieh et al. 2018; Wang et al. 2017). However, due to the wide band gap of TiO_2 (3.0–3.2 eV) and ZnO (3.2–3.3 eV), it can only absorb ultraviolet light ($\lambda < 400$ nm), which limits its photocatalytic ability to degrade pollutants in sunlight. Recently, the Bi-based semiconductor materials especially for bismuth oxyhalides have obtained more attention as photocatalysts (Chen et al. 2018b; Hao et al. 2019; Shi et al. 2019; Wang et al. 2018a) due to its intrinsic properties including distinct layered structure, harmless, low-priced and simple preparation method (Di et al. 2017; Jia et al. 2017). Among bismuth oxyhalides (BiOX; X = I, Cl, Br, and F), BiOI and BiOBr can absorb visible light of less than 430 nm and 630 nm, respectively, which would impart bright color to textiles (Di et al. 2017). BiOX (X = Br and I) also has a relatively high near-infrared reflectance, which makes it cool pigment (Gao et al. 2018).

In this work, the color adjustable solid solutions nanosheets formed with BiOBr and BiOI can be anchored on cotton fabric for photodegrading organic stain and absorbing ultraviolet light. Raw cotton was first carboxymethylated to adsorb $Bi_2O_2^{2+}$ to facilitate the growth of crystal nuclei. Subsequently, novel solid solution $BiOBr_xI_{1-x}$ nanosheets formed with different molar ratios of BiOBr and BiOI were anchored on carboxymethylated cotton fabric surface via the successive ionic layer adsorption and reaction methods (SILAR) (Zhou et al. 2019a). The structure and morphology of prepared multifunctional cotton fabrics ($BiOBr_xI_{1-x}$-CCF ($0 \leq x \leq 1$)) were characterized. Adjusted color, self-cleaning, UV protection, near-infrared reflectance, and acid and alkali resistance properties of these multifunctional cotton fabrics were also systematically studied.

Experimental section

Materials

Woven cotton (155 g/m^2) was purchased from Hua Fang Co., LTD. Bismuth nitrate pentahydrate ($Bi(NO_3)_3{\cdot}5H_2O$) anhydrous ethanol, chloroacetic acid, rhodamine B (RhB), potassium bromide (KBr), and potassium iodide (KI) were purchased from Adamas-beta Co., Ltd. The water used in the experiment is ultrapure water. All chemicals are of analytical grade.

Preparation of $BiOBr_xI_{1-x}$-CCF

To facilitate the nucleation of solid solution $BiOBr_xI_{1-x}$ nanosheets, cotton fabric was first modified by chloroacetic acid to achieve available carboxylates (Rubin et al. 2018; Wu et al. 2017). Subsequently, carboxymethylated cotton fabric (CCF) was used to electrostatically adsorb bismuth oxygen ions ($Bi_2O_2^{2+}$) in $Bi(NO_3)_3$ solution and then reacted with iodide and bromide ions in mixed solutions of KBr and KI with different molar ratios (Cai et al. 2018; Zhou et al. 2019a) (Scheme 1). The specific experimental details including carboxymethylation of cotton and growth process of solid solution nanosheets were placed in supplementary material. Prepared samples were defined as $BiOBr_xI_{1-x}$-CCF (x = n(KBr)/n(KBr+KI); x = 0, 0.2, 0.4, 0.6, 0.8, and 1).

Characterization

The morphology and microstructure of the treated cotton were investigated by SEM, TM-1000, Hitachi, Japan and FE-SEM; Hitachi, S-4800, Japan. Infrared spectra of raw cotton fabric and CCF were investigated with a perkinElmer spectrum-two (USA). The X-ray powder diffraction (XRD) patterns were performed on Rigaku D/max-2500PC, Cu Kα (λ = 1.54056 Å) (reflection mode). Raman spectra were collected on Thermo Fisher DXR2xi exciting with a 532.0 nm laser. X-ray photoelectron spectroscopy (XPS) were obtained on Thermo ESCALAB 250. UV-vis diffuse reflection spectrum (UV-vis DRS) and near infrared reflectance (NIR) spectroscopy were achieved on UV 3600PLUS. CIE 1976 L*a*b* colorimetric method was used to represent the color parameters of the samples. Color parameters were obtained from DATACOLOR 650. The UV blocking of the samples were tested by Fabric UV Transmittance Tester (UV-1000F). Contact angle was tested on a Theta contact angle analyzer (Biolin, Sweden).

Results and discussion

Structure and morphology

In order to increase loading efficiency of BiOX (X = Br or I) nanosheets on the cotton surface, the

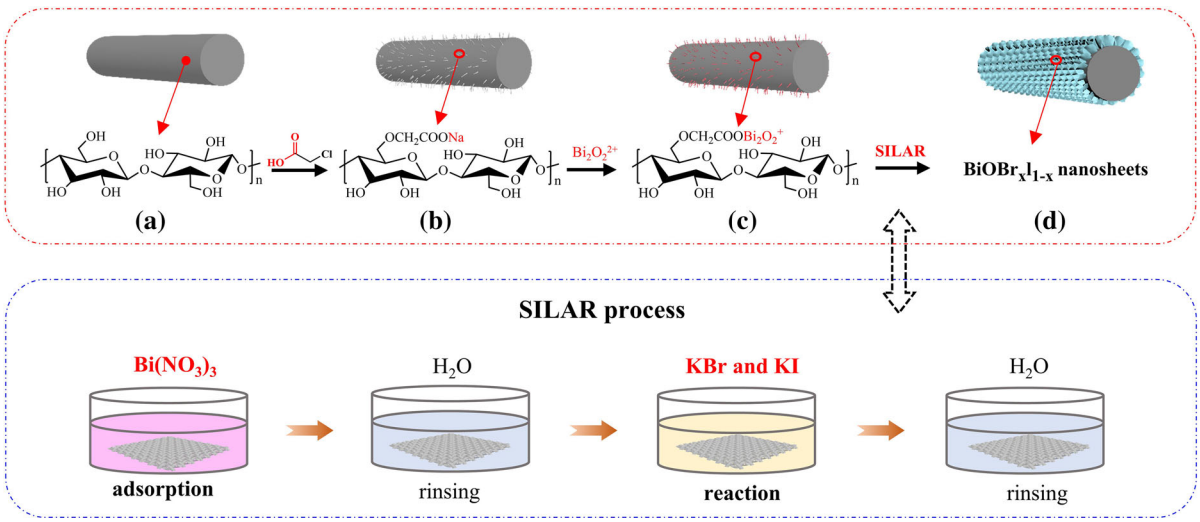

Scheme 1 Schematic diagram of the preparation process of $BiOBr_xI_{1-x}$-CCF ($0 \leq x \leq 1$)

cotton fabric was first functionalized with carboxylate groups. IR spectroscopy and XRD patterns of raw cotton fabric and CCF were investigated to confirm the presence of carboxyl groups.

As displayed in Fig. 1a, the IR absorption peak at 1725 cm^{-1} of CCF was ascribed to carboxylate group because the sample for testing was in the cellulose –OCH_2COOH form, and protonated carboxylic group (–COOH) in CCF yielded a C=O band (Wu et al. 2017). Both raw cotton and CCF were presented in the form of fabrics for XRD test. As displayed in Fig. 1b, XRD peaks at 2θ = 15.14, 16.58, and 22.88° are ascribed to the (1–10), (110) and (200) peaks of the cellulose Iβ pattern. Compared with raw cotton, XRD intensities of CCF at 2θ = 20.5° for the (012) and (102) increase, which means that the modification makes some crystallites on the fiber surface change from preferred orientation to random orientation (French 2014). The carboxyl concentration (C_{COO}−) on the modified cotton is 1.4 mmol/g and this material was used to prepare multifunctional $BiOBr_xI_{1-x}$-CCF.

The contents of BiOX (X = Br or I) loaded on raw cotton and CCF were tested and the results showed the content of the BiOX on CCF is higher than that of raw cotton (Table S1), which is attributed to coulombic force between $Bi_2O_2^{2+}$ in the solution and carboxyl groups on CCF (Tolba et al. 2017; Zhou et al. 2019b). Structure and morphology of prepared $BiOBr_xI_{1-x}$-CCF ($0 \le x \le 1$) were investigated to confirm the existence of solid solution $BiOBr_xI_{1-x}$ nanosheets.

As displayed in Fig. 2a, the significant XRD peaks of $BiOBr_xI_{1-x}$-CCF (x = 0) at 2θ = 9.36, 29.44, 31.54, 45.46, and 55.12 were attributed to tetragonal BiOI, which correspond to crystal faces of the (001), (102), (110), (200), and (212) peaks, respectively (Wang et al. 2010; Zhou et al. 2019a), and the significant XRD peaks of $BiOBr_xI_{1-x}$-CCF (x = 1) at 2θ = 10.92, 25.20, 32.24, 46.21, and 57.21° were ascribed to tetragonal BiOBr, which correspond to crystal faces of the (001), (101), (110), (200), and (212) peaks, respectively (Huo et al. 2012; Li et al. 2018). As for $BiOBr_xI_{1-x}$-CCF ($0 < x < 1$), the XRD pattern of prepared sample is a mixture pattern of BiOI-CCF and BiOBr-CCF, which is because the solid solution $BiOBr_xI_{1-x}$ ($0 < x < 1$) nanosheets consists of BiOI and BiOBr (Cao et al. 2011; Tang et al. 2016; Wang et al. 2018a). As displayed in Fig. 2b, the Raman scattering peaks of $BiOBr_xI_{1-x}$-CCF (x = 0) at 85.4 and 118.4 are ascribed to the A_{1g} (internal Bi-I stretching) and E_g (internal Bi-I stretching mode) of BiOI and the Raman scattering peaks of $BiOBr_xI_{1-x}$-CCF (x = 1) at 119 and 159 cm^{-1} are ascribed to the A_{1g} (internal Bi–Br stretching) and E_g (internal Bi-Br stretching mode) of BiOBr. Also, as for $BiOBr_xI_{1-x}$-CCF ($0 < x < 1$), the Raman scattering peaks of prepared sample is a mixture pattern of BiOI-CCF and BiOBr-CCF (Tian et al. 2012; Zhang et al. 2012). Based on the above results, the solid solution formed with different molar ratio of BiOI and BiOBr was anchored on the surface of cotton fabric.

From the low-magnification electron micrograph in Fig. 3a–f, it can be found that cotton fabric is completely covered by $BiOBr_xI_{1-x}$ ($0 \le x \le 1$). As displayed in Fig. 3a′–f′, $BiOBr_xI_{1-x}$ ($0 \le x \le 1$)

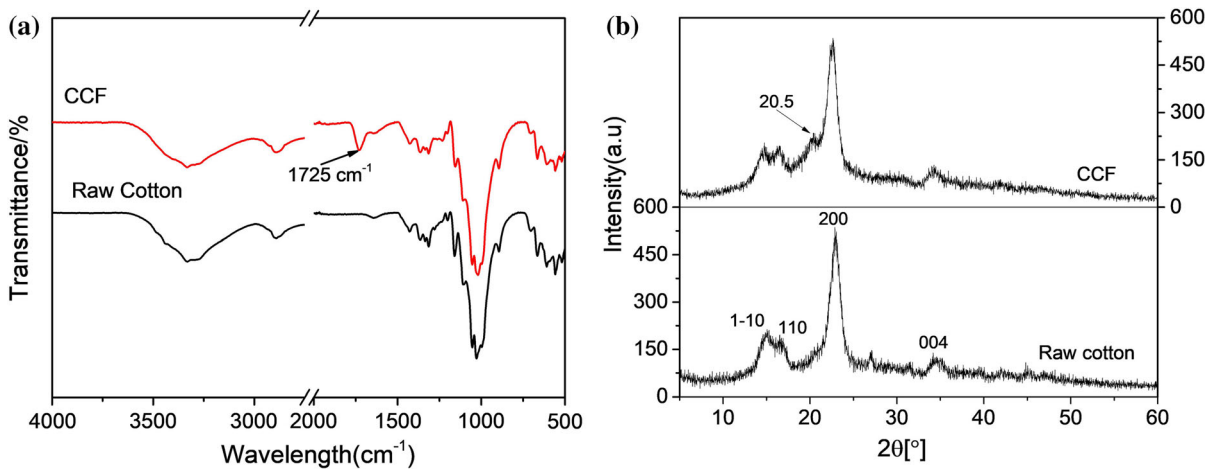

Fig. 1 **a** IR spectroscopy, **b** XRD patterns of raw cotton and CCF

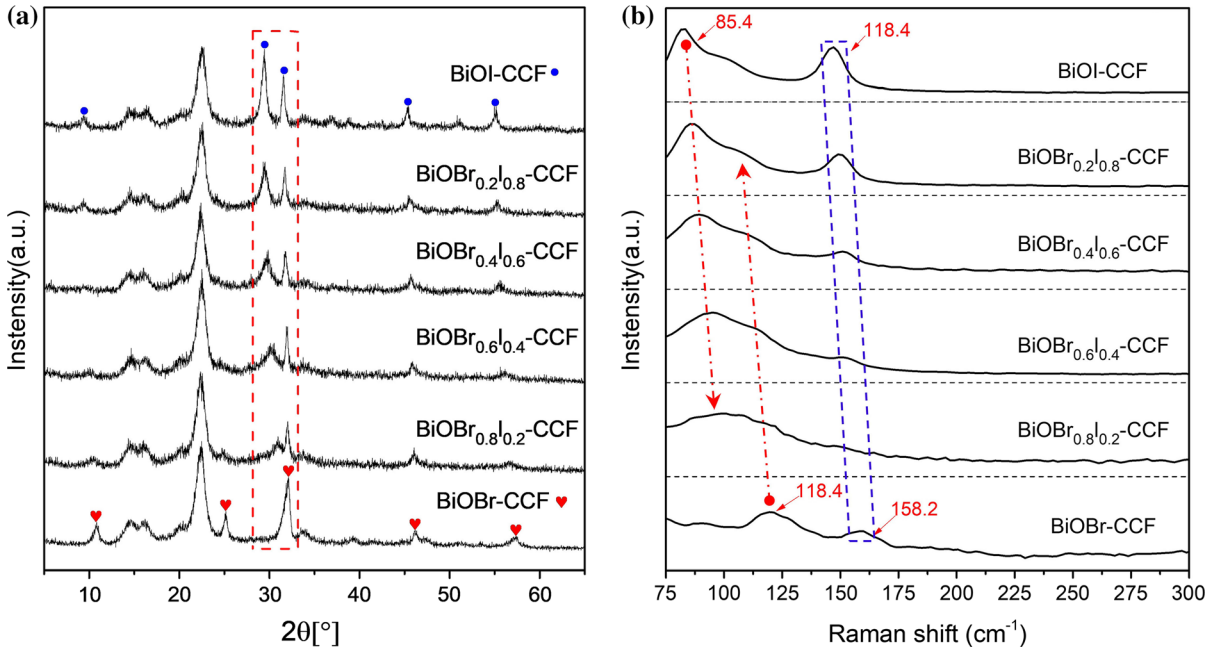

Fig. 2 **a** XRD patterns, **b** Raman scattering patterns of $BiOBr_xI_{1-x}$-CCF ($0 \le x \le 1$)

formed with different molar ratio of BiOI and BiOBr is in the form of a nanosheet. From the illustration in Fig. 3a′, f′, the average thickness of the nanosheet is 40–50 nm and a size of the nanosheet is 1–2 μm in the other two dimensions (Xia et al. 2011; Zhang et al. 2013). With the increase of bromide ion content, the nanosheets changed from interlaced arrangement to clustered flower-like (Cai et al. 2018; Huang et al. 2017a; Jia et al. 2017).

The elemental composition of $BiOBr_xI_{1-x}$-CCF ($0 \le x \le 1$) was tested and displayed in Fig. 4. As displayed in Fig. 4b, iodine is from BiOI and the peaks at 630.4 eV and 618.9 eV are ascribed to I $3d_{3/2}$ and I $3d_{5/2}$, respectively (Wang et al. 2016). As displayed in Fig. 4c, bromine is from BiOBr and the peaks at 69.3 eV and 68.3 eV are ascribed to Br $3d_{3/2}$ and $3d_{5/2}$, respectively. As for $BiOBr_xI_{1-x}$-CCF ($0 < x < 1$), XPS survey spectra exhibited the existence of Bi, O, I, Br, and C-related peaks, which is due to the co-existence of BiOX (X = I, Br) and cellulose. Bi-related peaks in all samples are attributed to the solid solution $BiOBr_xI_{1-x}$ nanosheets formed with BiOBr and BiOI. In Fig. 4d, the peaks of Bi 4*f* at 159.3 and 164.6 eV confirm the valence state of Bi^{3+} (Yu et al. 2017). In Fig. 4e, the peaks at 532.2 eV and 530.1 eV are mainly attributed to the surface absorbed oxygen and lattice oxygen.

Optical performance

For textile materials, bright colors help to enhance the appreciation and added value of products. As displayed in Fig. 5a, by regulating the molar ratio of bromine ions to iodide ions in mixed solution, a series of colored fabrics ($BiOBr_xI_{1-x}$-CCF) were obtained (Lu et al. 2018; Wang et al. 2018a). Color coordinates of $BiOBr_xI_{1-x}$-CCF ($0 \le x \le 1$) were listed in Table 1. With the increase of iodine ion content, the lightness (L) of $BiOBr_xI_{1-x}$-CCF decreases, and a* (green(−)/red(+)) value decreases first and then increases, which is opposite to that of b* (blue(−)/yellow(+)) value. With the increase of iodine ion content, the color of the composite fabrics ($BiOBr_xI_{1-x}$-CCF) changes from white to yellow and finally to red. As displayed in Fig. 3b, the chromaticity coordinates of $BiOBr_xI_{1-x}$-CCF ($0 \le x \le 1$) were drawn in the CIE two-dimensional chromaticity diagram. As shown in the Fig. 5b, if the molar ratio of bromine to iodine is refined, a chromaticity coordinate curve can be obtained.

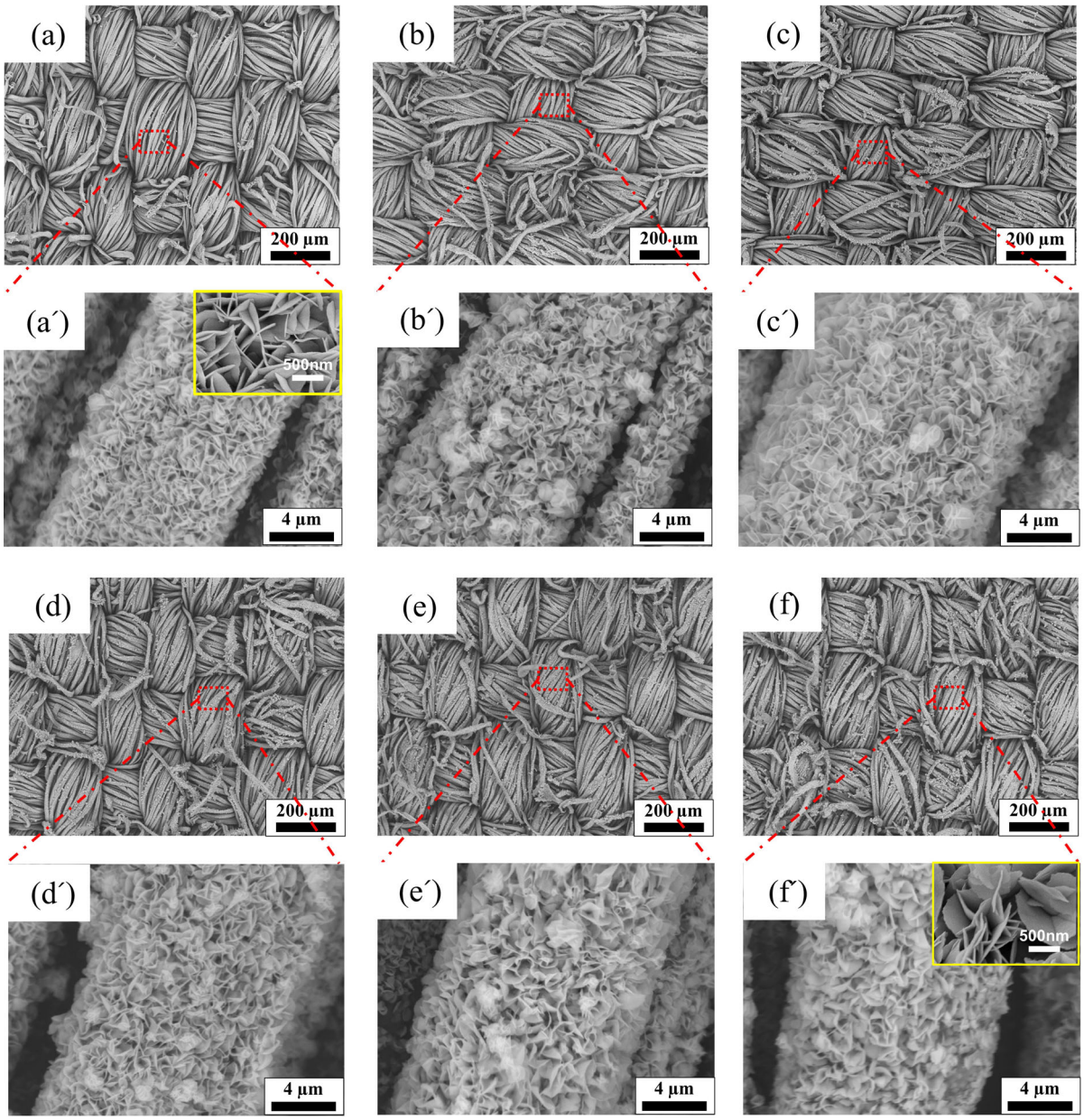

Fig. 3 SEM images of $BiOBr_xI_{1-x}$-CCF (**a**, **a´**: x = 0; **b**, **b´**: x = 0.2; **c**, **c´**: x = 0.4; **d**, **d´**: x = 0.6; **e**, **e´**: x = 0.8; **f**, **f´**: x = 1)

The color is related to the optical absorption of the composite fabric and the optical absorption of the composite fabric ($BiOBr_xI_{1-x}$-CCF) is mainly decided by the band structure of the solid solution $BiOBr_xI_{1-x}$ nanosheets. As displayed in Fig. 5c, with the increase of iodine content, the absorption edge of $BiOBr_xI_{1-x}$-CCF ($0 \leq x \leq 1$) was extended from 430 nm to 630 nm. Band gap of composite fabrics ($BiOBr_xI_{1-x}$-CCF) were calculated (Bai et al. 2019; Wang et al. 2018b) and specific method was placed in supplementary material (Fig. S1). The results were listed in Table 1. With the increase of iodine ion content, band gap of $BiOBr_xI_{1-x}$-CCF gradually decreases from 2.71 to 1.85 eV.

Studies have shown that ultraviolet light can cause a series of skin diseases and it is also an important cause of facial aging (Schuch et al. 2017). As an important textile material for clothes and industry, UV

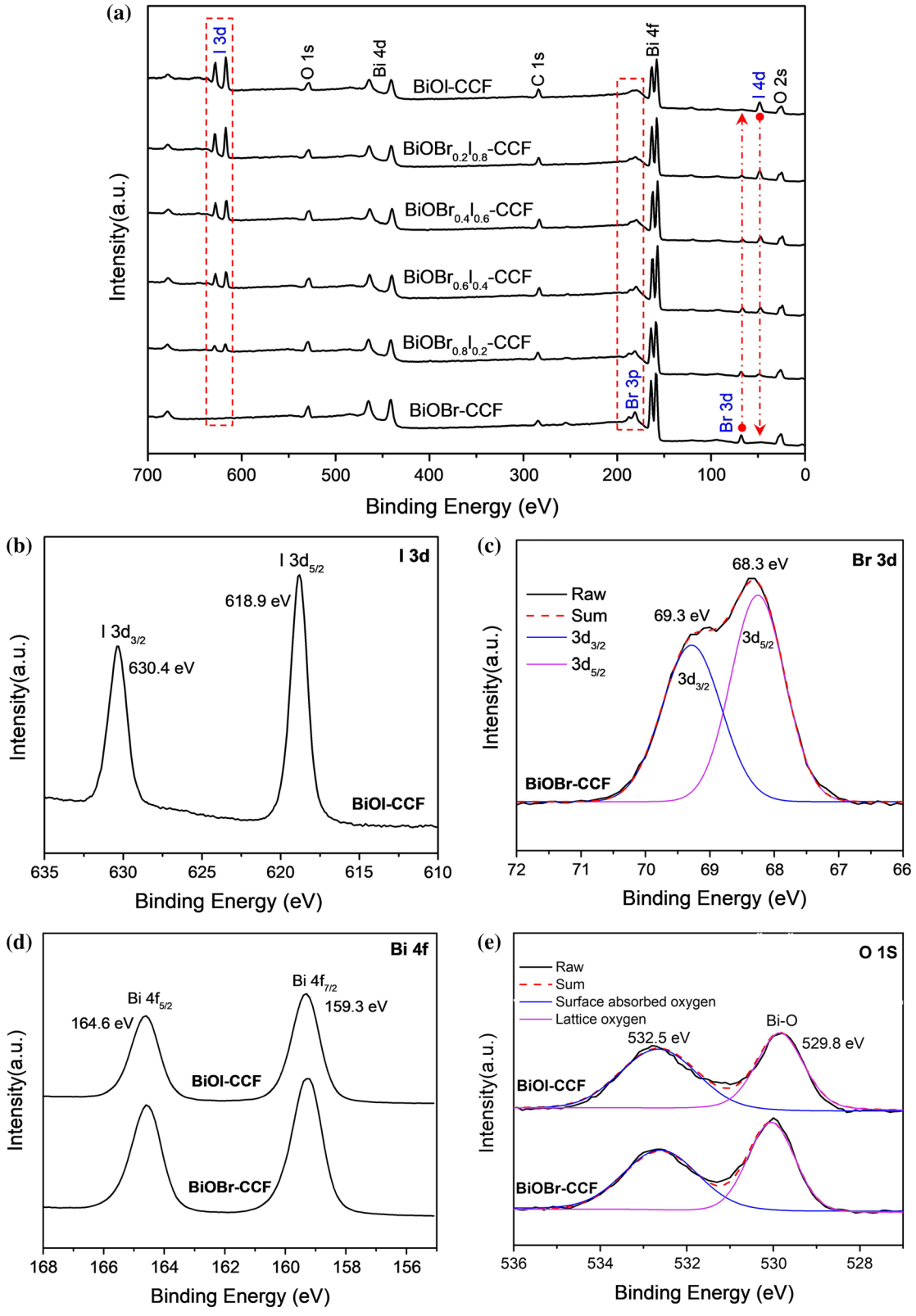
(a)
I 3d
O 1s
Bi 4d
C 1s
Bi 4f
I 4d
O 2s
BiOI-CCF
BiOBr0.2I0.8-CCF
BiOBr0.4I0.6-CCF
BiOBr0.6I0.4-CCF
BiOBr0.8I0.2-CCF
BiOBr-CCF
Br 3p
Br 3d
Intensity(a.u.)
Binding Energy (eV)
(b)
I 3d
I 3d5/2
618.9 eV
I 3d3/2
630.4 eV
BiOI-CCF
Intensity(a.u.)
Binding Energy (eV)
(c)
Br 3d
68.3 eV
Raw
Sum
3d3/2
3d5/2
69.3 eV
3d5/2
3d3/2
BiOBr-CCF
Intensity(a.u.)
Binding Energy (eV)
(d)
Bi 4f
Bi 4f5/2
164.6 eV
Bi 4f7/2
159.3 eV
BiOI-CCF
BiOBr-CCF
Intensity(a.u.)
Binding Energy (eV)
(e)
O 1S
Raw
Sum
Surface absorbed oxygen
Lattice oxygen
Bi-O
532.5 eV
529.8 eV
BiOI-CCF
BiOBr-CCF
Intensity(a.u.)
Binding Energy (eV)

◀**Fig. 4** **a** XPS survey spectra of $BiOBr_xI_{1-x}$-CCF ($0 \le x \le 1$); High-resolution XPS spectrums of I 3*d* (**b**), Br 3*d* (**c**), Bi 4*f* (**d**) and O 1*s* (**e**)

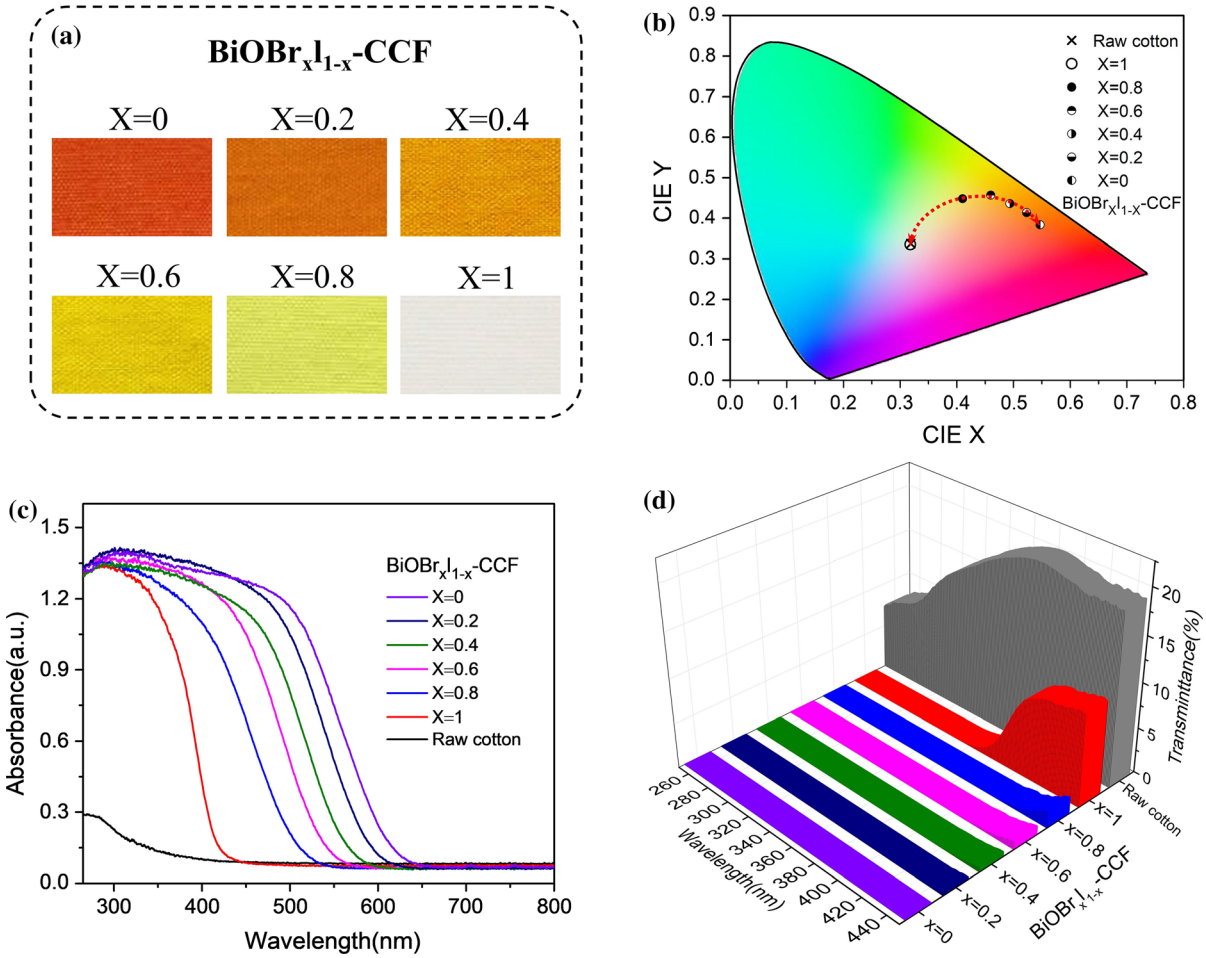

Fig. 5 **a** Digital photos of $BiOBr_xI_{1-x}$-CCF ($0 \le x \le 1$), **b** CIE two-dimensional chromaticity diagram of raw cotton and $BiOBr_xI_{1-x}$-CCF ($0 \le x \le 1$), **c** UV–Vis DRS of raw cotton and $BiOBr_xI_{1-x}$-CCF, **d** UV transmission rate of raw cotton and $BiOBr_xI_{1-x}$-CCF ($0 \le x \le 1$)

protection of cotton fabric is concerned (Chen et al. 2018a; Ma et al. 2019). As displayed in Fig. 5d, the ultraviolet transmittance (250–450 nm) of raw cotton is much higher than that of $BiOBr_xI_{1-x}$-CCF ($0 \le x \le 1$). As the iodine content increases, the UV transmittance of $BiOBr_xI_{1-x}$-CCF gradually decreases, but the magnitude of the change is small. UV protection can be expressed as a numerical value of UV protection factor (UPF). Transmittance percentages (UV-A and UV-B) and UPF of raw cotton and $BiOBr_xI_{1-x}$-CCF can be calculated according to the following formulas (Zhou et al. 2019a).

$$T(UV-A) = \frac{\sum_{315\ nm}^{400\ nm} T_\lambda \Delta_\lambda}{\sum_{315\ nm}^{400\ nm} \Delta_\lambda} \quad (1)$$

$$T(UV-B) = \frac{\sum_{280\ nm}^{315\ nm} T_\lambda \Delta_\lambda}{\sum_{280\ nm}^{315\ nm} \Delta_\lambda} \quad (2)$$

$$UPF = \frac{\sum_{280\ nm}^{400\ nm} E_\lambda S_\lambda \Delta_\lambda}{\sum_{280\ nm}^{400\ nm} E_\lambda S_\lambda T_\lambda \Delta_\lambda} \quad (3)$$

Table 1 Color coordinates and band gap of $BiOBr_xI_{1-x}$-CCF ($0 \leq x \leq 1$)

Samples	CIE L	CIE a	CIE b	Band gap (eV)
Raw cotton	94.67	− 0.07	2.39	–
BiOBr-CCF	93.38	− 0.60	3.25	2.71
$BiOBr_{0.8}I_{0.2}$-CCF	91.05	− 5.34	61.69	2.24
$BiOBr_{0.6}I_{0.4}$-CCF	85.35	8.77	77.93	2.11
$BiOBr_{0.4}I_{0.6}$-CCF	78.17	24.71	75.91	2.01
$BiOBr_{0.2}I_{0.8}$-CCF	68.62	38.09	67.83	1.93
BiOI-CCF	58.58	44.60	54.25	1.85

where E_λ, S_λ, T_λ, and Δ_λ are the relative erythemal spectral effectiveness, solar spectral irradiance, average spectral transmission of the specimen, and measured wavelength interval (nm), respectively.

As listed in Table 2, the UV protection of raw cotton is weak (UPF < 10). Compare with raw cotton, UPF of $BiOBr_xI_{1-x}$-CCF ($0 \leq x \leq 1$) is 50+ and its T(UV-A) is less than 5%, which is ascribed to the strong ultraviolet absorption ability of $BiOBr_xI_{1-x}$ nanosheets (Zhou et al. 2019a). According to GB/T18830-2009, $BiOBr_xI_{1-x}$-CCF ($0 \leq x \leq 1$) can be used as "UV protection product".

Self-cleaning performance

Awning and decorative fabrics generally need to have self-cleaning properties. Self-cleaning of textiles mainly includes two features (Banerjee et al. 2015). First, textiles are not easily stained by stains. To facilitate the observation of the staining effect, a colored aqueous solution was used to test the staining effect of the fabrics (raw cotton and $BiOBr_xI_{1-x}$-CCF (x = 1)). As displayed in Fig. 6a, raw cotton was easily stained by the colored aqueous solution, while $BiOBr_xI_{1-x}$-CCF (x = 1) were not easily stained by the colored aqueous solution. Contact angles between the water and the surface of raw cotton and $BiOBr_xI_{1-x}$-CCF also were tested. As displayed in Fig. 6b, water was easily spread on cotton fabrics and is not easily spread on $BiOBr_xI_{1-x}$-CCF ($0 \leq x \leq 1$). This result can be attributed to two factors: (1) The solid solution is a crystal sheet which is insoluble in water; (2) The cross-arranged $BiOBr_xI_{1-x}$ nanosheets on cotton fiber surface have a "lotus-like effect". The contact angles between $BiOBr_xI_{1-x}$-CCF ($0 \leq x \leq 1$) and water range from 139 to 143 degrees, which make $BiOBr_xI_{1-x}$-CCF ($0 \leq x \leq 1$) not easily stained by the water-based stains in life.

Table 2 Transmittance percentages (UV-A and UV-B) and UPF of raw cotton and $BiOBr_xI_{1-x}$-CCF ($0 \leq x \leq 1$)

Samples	T(UV-A)/%	T(UV-B)/%	UPF
Raw cotton	18.49	13.27	6.88
BiOBr-CCF	1.32	< 0.05	50+
$BiOBr_{0.8}I_{0.2}$-CCF	< 0.05	< 0.05	50+
$BiOBr_{0.6}I_{0.4}$-CCF	< 0.05	< 0.05	50+
$BiOBr_{0.4}I_{0.6}$-CCF	< 0.05	< 0.05	50+
$BiOBr_{0.2}I_{0.8}$-CCF	< 0.05	< 0.05	50+
BiOI-CCF	< 0.05	< 0.05	50+

Second, once textiles are stained, the stain can be effectively degraded (Chen et al. 2019; Huang et al. 2017b; Qin et al. 2019). The ability of $BiOBr_xI_{1-x}$-CCF ($0 \leq x \leq 1$) to photodegrade organic stain solution (Rh B) was tested under visible light irradiation (500 W xenon lamp, $\lambda > 400$ nm) and experimental details were placed in supplementary material. The results showed that all the samples ($BiOBr_xI_{1-x}$-CCF ($0 \leq x \leq 1$)) can photodegrade Rh B in aqueous solution. As displayed in Fig. 6c, with the increase of bromide ion content, the photodegradation effect of Rh B is gradually increasing and $BiOBr_xI_{1-x}$-CCF (x = 1) can photodegrade > 99% Rh B in 180 min. Photocatalytic decontamination of stains on the surface of raw cotton and $BiOBr_xI_{1-x}$-CCF (x = 1) was further simulated under visible light irradiation (500 W xenon lamp, $\lambda > 400$ nm). The $BiOBr_xI_{1-x}$-CCF (x = 1) was first wetted with a mixture of ethanol and water, and then the stain (10 mg/L Rh B solution) was dripped onto the surface of the fabric and illuminated by xenon lamp ($\sim$ 500 W; $\lambda > 400$ nm) to observe the color change of the stain (Valenzuela et al. 2019). As displayed in Fig. 6d, as the irradiation time was prolonged, the color of the stain on $BiOBr_xI_{1-x}$-CCF (x = 1) gradually faded, while the color of the stain on raw cotton hardly changed. These results indicate that $BiOBr_xI_{1-x}$-CCF has the ability to photodegrade stain. Therefore, $BiOBr_xI_{1-x}$-CCF ($0 \leq x \leq 1$) can be used as self-cleaning textile.

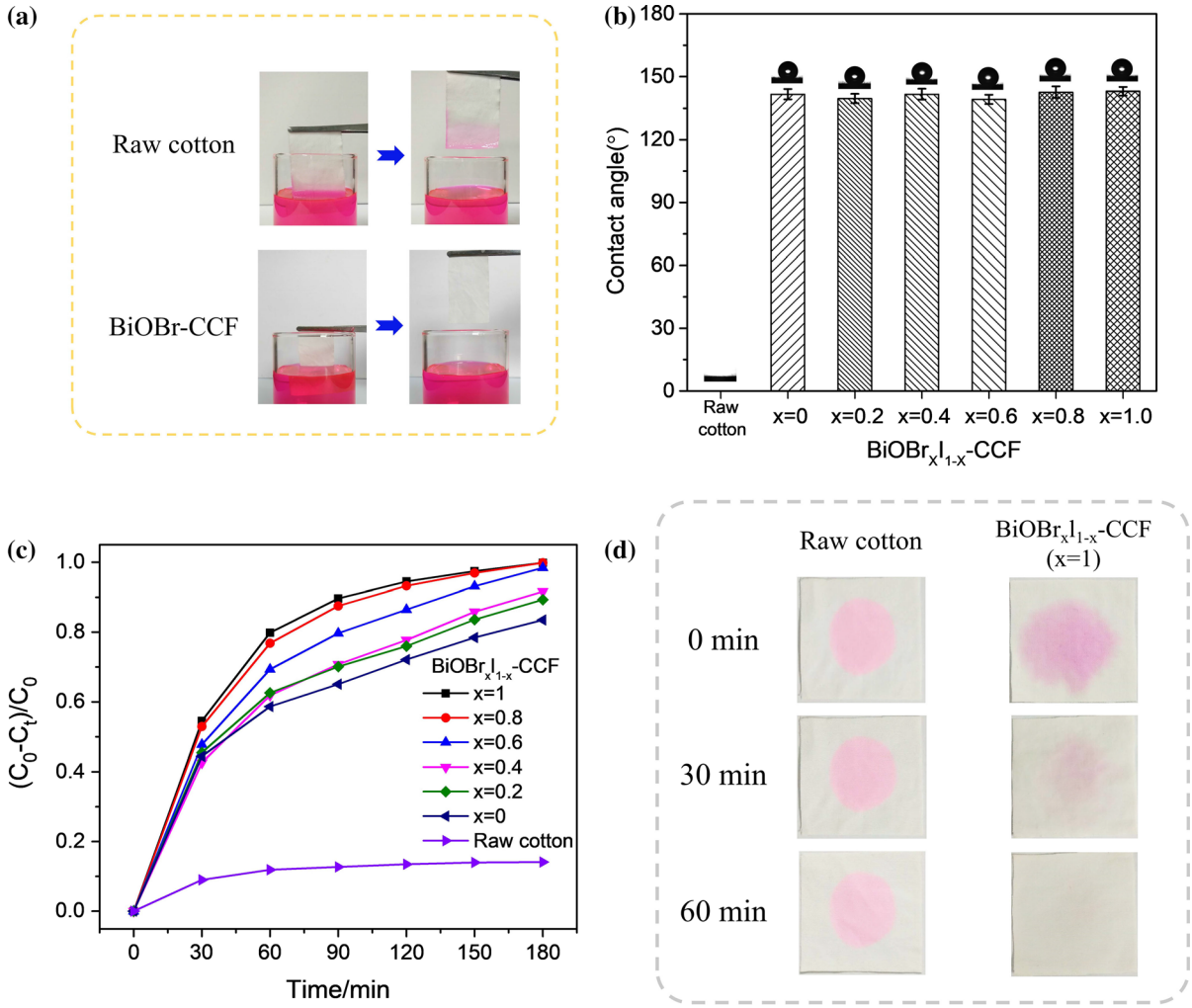

Fig. 6 **a** Wetting properties of raw cotton and $BiOBr_xI_{1-x}$-CCF (x = 1), **b** Contact angle between the water and the surface of raw cotton and $BiOBr_xI_{1-x}$-CCF ($0 \leq x \leq 1$), **c** Photodegrading Rh B in aqueous solution with $BiOBr_xI_{1-x}$-CCF ($0 \leq x \leq 1$) under visible light irradiation (500 W xenon lamp, $\lambda > 400$ nm), **d** Photocatalytic decontamination of Rh B on the surface of raw cotton and $BiOBr_xI_{1-x}$-CCF (x = 1) under visible light irradiation (500 W xenon lamp, $\lambda > 400$ nm)

NIR reflectance property

In tropical and subtropical regions, the near infrared reflection performance (700–2500 nm) of outdoor tents and curtains is critical for thermal isolation. Photocatalysts can be used as NIR reflective pigments (Gao et al. 2017; Lu et al. 2017).

As displayed in Fig. 7a, the near infrared reflectance of $BiOBr_xI_{1-x}$-CCF ($0 \leq x \leq 1$) is higher than that of raw cotton without photocatalyst, which is attributed to the near-infrared reflection properties of the solid solution $BiOBr_xI_{1-x}$ nanosheets. The near infrared reflectance of $BiOBr_xI_{1-x}$-CCF ($0 \leq x \leq 1$) has no linear relationship with the ratio of bromine to iodine. As displayed in Fig. 7b, the samples ($BiOBr_x$-I_{1-x}-CCF) were placed on a plate made of foil paper and polystyrene foam under an infrared lamp (Philips BR 250 W) (Gao et al. 2018). The outer surface temperature and thermography images of raw cotton of $BiOBr_xI_{1-x}$-CCF were obtained by a forward-looking infrared radiometer IR imaging camera (FLK-TIR329HZ, Fluke, USA). As displayed in Fig. 7c–i, the surface temperature of $BiOBr_xI_{1-x}$-CCF ($0 \leq x \leq 1$) is lower than that of raw cotton, which is attributed to near infrared reflectance of solid solution $BiOBr_xI_{1-x}$ nanosheets. From the Fig. 7a and c–i, it

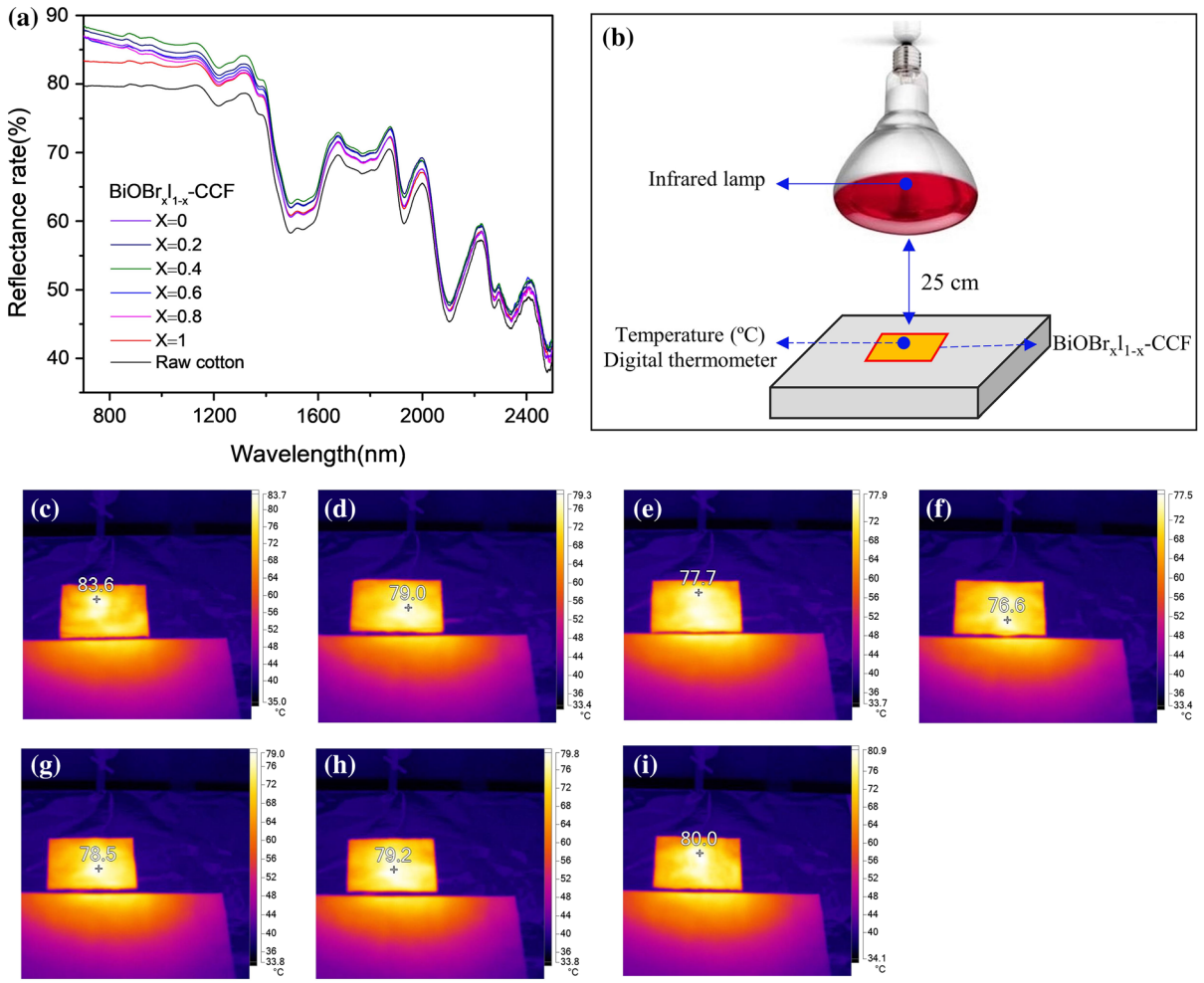

Fig. 7 **a** NIR reflectance of $BiOBr_xI_{1-x}$-CCF ($0 \leq x \leq 1$), **b** A simple device used for testing the surface temperature of $BiOBr_xI_{1-x}$-CCF ($0 \leq x \leq 1$); Thermography image of raw cotton (**c**) and $BiOBr_xI_{1-x}$-CCF (**d**, x = 0; **e**, x = 0.2; **f**, x = 0.4; **g**, x = 0.6; **h**, x = 0.8; **i**, x = 1) (the sample size is 6.5×8 cm) under an infrared lamp (250 W)

can be found that the higher the near infrared reflectance of the sample, the lower its surface temperature. Among these Samples, $BiOBr_xI_{1-x}$-CCF (x = 0.4) has the highest near infrared light reflectivity and the lowest surface temperature under an infrared lamp irradiation. Therefore, $BiOBr_xI_{1-x}$-CCF ($0 \leq x \leq 1$) can be used as infrared reflectance textile material.

Acid and alkali resistance

The solid solution $BiOBr_xI_{1-x}$ nanosheets on cotton fabric were regarded as inorganic pigments. The acid and alkali resistance of inorganic pigments is an important factor affecting its practical application and further functional finishing. In order to facilitate observing the change of the sample in acid/alkali solutions, colored $BiOBr_xI_{1-x}$-CCF (x = 0) was selected as the test sample and was placed in solution with different pH for 3 h.

As displayed in Fig. 8a, when $BiOBr_xI_{1-x}$-CCF (x = 0) was soaked in a solution with pH = 1.1 and 12.1, its color changes significantly, which means the structure of BiOI nanosheets has been destroyed. However, when $BiOBr_xI_{1-x}$-CCF (x = 0) was immersed in the solution with pH 2.3 and 11.2 for 3 h, there was no change in color. Soaked samples in pH 2.3 and 11.2 were characterized by SEM and X-ray powder diffraction. As displayed in Fig. 8b, c, there is no difference between the X-ray powder diffraction

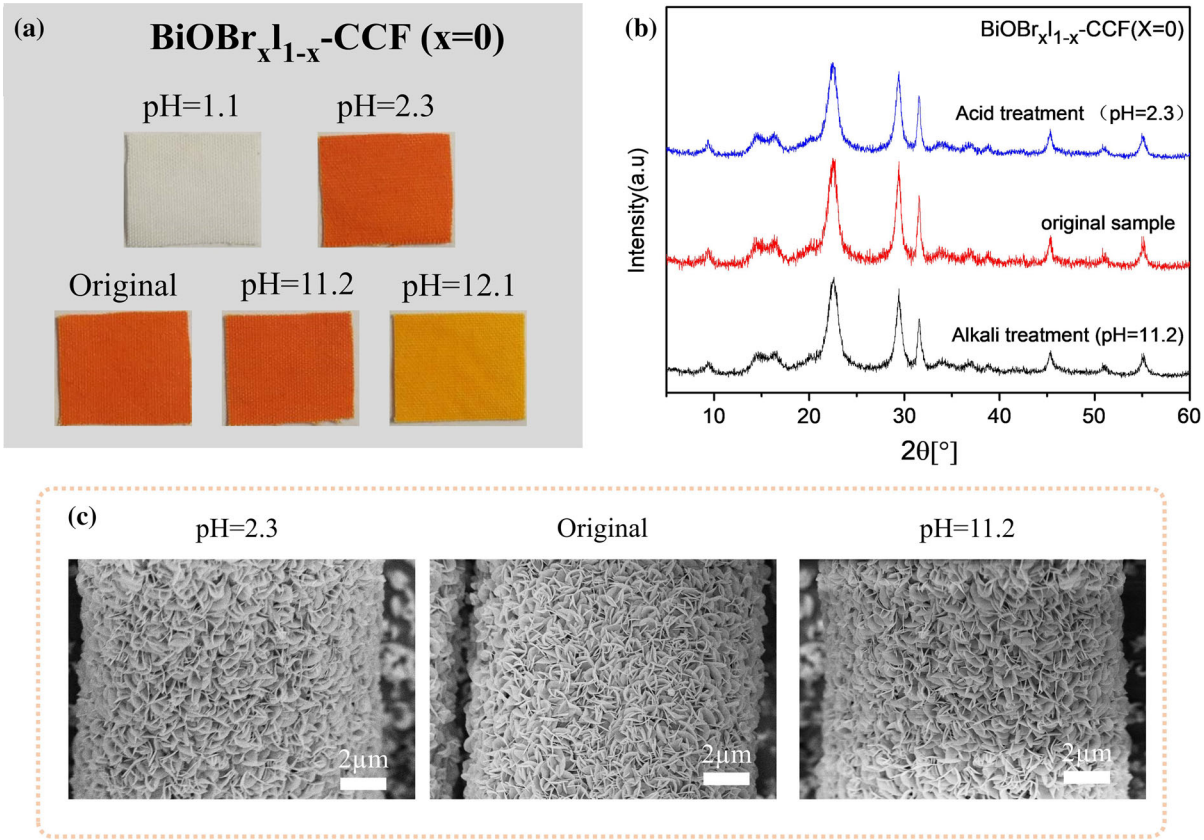

Fig. 8 **a** Digital photos of $BiOBr_xI_{1-x}$-CCF (x = 0) treated with acidic and alkaline solution, **b** X-ray powder diffraction patterns and **c** SEM of $BiOBr_xI_{1-x}$-CCF (x = 0) treated with acid/alkali solutions

peaks and the morphology of $BiOBr_xI_{1-x}$-CCF (x = 0) treated with acid/alkali solutions and the original sample. This result indicates that $BiOBr_xI_{1-x}$-CCF ($0 \le x \le 1$) has a certain acid and alkali resistance.

Conclusion

Multifunctional cotton fabric was simply fabricated by anchoring the solid solution $BiOBr_xI_{1-x}$ nanosheets formed with different molar ratios of BiOBr and BiOI on the carboxymethylated cotton fabric. The color of the composite fabrics ($BiOBr_xI_{1-x}$-CCF) can be adjusted. The solid solution nanosheets formed with different molar ratios of BiOBr and BiOI impart the self-cleaning, excellent UV protection (UPF > 50, T(UV-A) < 5%), and NIR reflective properties to cotton fabrics. These multifunctional cotton fabrics ($BiOBr_xI_{1-x}$-CCF) have great potential usage in self-cleaning and outdoor protection.

Acknowledgments This work is supported by the National Natural Science Foundation of China (No. 21872025) and the National Key R & D Program of China (No. 2017YFB0309700).

Funding The authors declare no financial interest.

References

Bai Y et al (2019) $BiOBr_xI_{1-x}$/BiOBr heterostructure engineering for efficient molecular oxygen activation. Chem Eng J 359:813. https://doi.org/10.1016/j.cej.2018.11.002

Banerjee S, Dionysiou DD, Pillai SC (2015) Self-cleaning applications of TiO_2 by photo-induced hydrophilicity and photocatalysis. Appl Catal B Environ 176:396–428. https://doi.org/10.1016/j.apcatb.2015.03.058

Cai Y, Song J, Liu X, Yin X, Li X, Yu J, Ding B (2018) Soft BiOBr@TiO_2 nanofibrous membranes with hierarchical heterostructures as efficient and recyclable visible-light

photocatalysts. Environ Sci Nano 5:2631–2640. https://doi.org/10.1039/c8en00866c

Cao J, Xu BY, Luo BD, Lin HL, Chen SF (2011) Novel BiOI/BiOBr heterojunction photocatalysts with enhanced visible light photocatalytic properties. Catal Commun 13:63–68. https://doi.org/10.1016/j.catcom.2011.06.019

Chen DZ et al (2018a) UV-blocking, superhydrophobic and robust cotton fabrics fabricated using polyvinyl-silsesquioxane and nano-TiO_2. Cellulose 25:3635–3647. https://doi.org/10.1007/s10570-018-1790-7

Chen F, Huang HW, Ye LQ, Zhang TR, Zhang YH, Han XP, Ma TY (2018b) Thickness-dependent facet junction control of layered $BiOIO_3$ single crystals for highly efficient CO_2 photoreduction. Adv Funct Mater 28:11. https://doi.org/10.1002/adfm.201804284

Chen F, Huang HW, Guo L, Zhang YH, Ma TY (2019) The role of polarization in photocatalysis. Angew Chem Int Edition 58:10061–10073. https://doi.org/10.1002/anie.201901361

Di J, Xia J, Li H, Guo S, Dai S (2017) Bismuth oxyhalide layered materials for energy and environmental applications. Nano Energy 41:172–192. https://doi.org/10.1016/j.nanoen.2017.09.008

French AD (2014) Idealized powder diffraction patterns for cellulose polymorphs. Cellulose 21:885–896. https://doi.org/10.1007/s10570-013-0030-4

Gao Q, Wu X, Xia Z, Fan Y (2017) Coating mechanism and near-infrared reflectance property of hollow fly ash bead/TiO_2 composite pigment. Powder Technol 305:433–439. https://doi.org/10.1016/j.powtec.2016.10.037

Gao Q, Wu XM, Lu DH, Fan YM (2018) Optical property and thermal performance of hollow glass microsphere/BiOBr 1-xIx composites as a novel colored near infrared reflective pigment. Dyes Pigments 154:21–29. https://doi.org/10.1016/j.dyepig.2018.02.038

Ge B et al (2018) Fabrication of superhydrophobic Cu–BiOBr surface for oil/water separation and water soluble pollutants degradation. Appl Surf Sci 462:583–589. https://doi.org/10.1016/j.apsusc.2018.08.174

Ge B et al (2020) A durable superhydrophobic BiOBr/PFW cotton fabric for visible light response degradation and oil/water separation performance. Colloids Surf A Physicochem Eng Asp 585:124027. https://doi.org/10.1016/j.colsurfa.2019.124027

Hao L et al (2019) Surface-halogenation-induced atomic-site activation and local charge separation for superb CO_2 photoreduction. Adv Mater 31:7. https://doi.org/10.1002/adma.201900546

Hu JT et al (2018) Functionalization of cotton fabrics with highly durable polysiloxane-TiO2 hybrid layers: potential applications for photo-induced water-oil separation, UV shielding, and self-cleaning. J Mater Chem A 6:6085–6095. https://doi.org/10.1039/c7ta11231a

Huang H, Xiao K, Du X, Zhang Y (2017a) Vertically aligned nanosheets-array-like BiOI homojunction: three-in-one promoting photocatalytic oxidation and reduction abilities. ACS Sustain Chem Eng 5:5253–5264. https://doi.org/10.1021/acssuschemeng.7b00599

Huang HW, Tu SC, Zeng C, Zhang TR, Reshak AH, Zhang YH (2017b) Macroscopic polarization enhancement promoting photo- and piezoelectric-induced charge separation and molecular oxygen activation. Angew Chem Int Edition 56:11860–11864. https://doi.org/10.1002/anie.201706549

Huo Y, Zhang J, Miao M, Jin Y (2012) Solvothermal synthesis of flower-like BiOBr microspheres with highly visible-light photocatalytic performances. Appl Catal B Environ 111:334–341

Jia H, Zhang B, He W, Xiang Y, Zheng Z (2017) Mechanistic insights into the photoinduced charge carrier dynamics of BiOBr/CdS nanosheet heterojunctions for photovoltaic application. Nanoscale 9:3180–3187. https://doi.org/10.1039/C6NR09259D

Li Y, Zhu J, Yang R, Shao M (2018) Facile synthesis of Bi decorated 2D and 3D BiOBr micro-nanostructures with enhanced photocatalytic activity. Iet Micro Nano Lett 13:1040–1045

Lu D, Gao Q, Wu X, Fan Y (2017) ZnO nanostructures decorated hollow glass microspheres as near infrared reflective pigment. Ceram Int 43:9164–9170. https://doi.org/10.1016/j.ceramint.2017.04.067

Lu JL et al (2018) Synthesis of visible-light-driven $BiOBr_xI_{1-x}$ solid solution nanoplates by ultrasound-assisted hydrolysis method with tunable bandgap and superior photocatalytic activity. J Alloys Compd 732:167–177. https://doi.org/10.1016/j.jallcom.2017.10.175

Ma W, Li L, Ren XH, Huang TS (2019) Rational design of cotton substrates with enhanced UV-blocking, high antibacterial efficiency and prominent hydrophobicity. Cellulose 26:5757–5768. https://doi.org/10.1007/s10570-019-02455-4

Moridi MZ, Shekarriz S, Afshar TF, Montazer M (2018) A new method for in situ synthesis of Ag–TiO_2 nanocomposite particles on polyester/cellulose fabric by photoreduction and self-cleaning properties. Cellulose 25:2355–2366. https://doi.org/10.1007/s10570-018-1694-6

Qin Q et al (2019) Waste cotton fiber/Bi_2WO_6 composite film for dye removal. Cellulose 26:3909–3922. https://doi.org/10.1007/s10570-019-02345-9

Rubin HN, Neufeld BH, Reynolds MM (2018) Surface-anchored metal-organic framework-cotton material for tunable antibacterial copper delivery. ACS Appl Mater Interfaces 10:15189–15199. https://doi.org/10.1021/acsami.7b19455

Schuch AP, Moreno NC, Schuch NJ, Menck CFM, Garcia CCM (2017) Sunlight damage to cellular DNA: focus on oxidatively generated lesions. Free Radic Biol Med 107:110–124. https://doi.org/10.1016/j.freeradbiomed.2017.01.029

Shi X, Wang PQ, Wang L, Bai Y, Xie HQ, Zhou Y, Ye LQ (2019) Change in photocatalytic NO removal mechanisms of ultrathin BiOBr/BiOI via NO_3^- adsorption. Appl Catal B Environ 243:322–329. https://doi.org/10.1016/j.apcatb.2018.10.037

Tang ZK, Yin WJ, Zhang L, Wen B, Zhang DY, Liu LM, Lau WM (2016) Spatial separation of photo-generated electron-hole pairs in BiOBr/BiOI bilayer to facilitate water splitting. Sci Rep 6:9. https://doi.org/10.1038/srep32764

Tian Y, Guo CF, Guo YJ, Wang Q, Liu Q (2012) BiOCl nanowire with hierarchical structure and its Raman features. Appl Surf Sci 258:1949–1954. https://doi.org/10.1016/j.apsusc.2011.06.137

Tolba AA, Mohamady SI, Hussin SS, Akashi T, Sakai Y, Galhoum AA, Guibal E (2017) Synthesis and characterization of poly(carboxymethyl)-cellulose for enhanced La(III) sorption. Carbohydr Polym 157:1809–1820. https://doi.org/10.1016/j.carbpol.2016.11.064

Valenzuela L, Iglesias A, Faraldos M, Bahamonde A, Rosal R (2019) Antimicrobial surfaces with self-cleaning properties functionalized by photocatalytic ZnO electrosprayed coatings. J Hazard Mater 369:665–673. https://doi.org/10.1016/j.jhazmat.2019.02.073

Wang K, Jia F, Zheng Z, Zhang L (2010) Crossed BiOI flake array solar cells. Electrochem Commun 12:1764–1767. https://doi.org/10.1016/j.elecom.2010.10.017

Wang K, Shao C, Li X, Miao F, Lu N, Liu Y (2016) Room temperature immobilized BiOI nanosheets on flexible electrospun polyacrylonitrile nanofibers with high visible-light photocatalytic activity. J Sol-Gel Sci Technol 80:783–792. https://doi.org/10.1007/s10971-016-4161-6

Wang Y et al (2017) Layer-by-layer self-assembly photocatalytic nanocoating on cotton fabrics as easily recycled photocatalyst for degrading gas and liquid pollutants. Cellulose 24:4569–4580. https://doi.org/10.1007/s10570-017-1445-0

Wang Q, Liu Z, Liu D, Liu G, Yang M, Cui F, Wang W (2018a) Ultrathin two-dimensional $BiOBr_xI_{1-x}$ solid solution with rich oxygen vacancies for enhanced visible-light-driven photoactivity in environmental remediation. Appl Catal B Environ 236:222–232. https://doi.org/10.1016/j.apcatb.2018.05.029

Wang Y, Long Y, Yang ZQ, Zhang D (2018b) A novel ion-exchange strategy for the fabrication of high strong BiOI/BiOBr heterostructure film coated metal wire mesh with tunable visible-light-driven photocatalytic reactivity. J Hazard Mater 351:11–19. https://doi.org/10.1016/j.jhazmat.2018.02.027

Wu Z, Zhou P, Yang J, Li J (2017) Determination of the optimal reaction conditions for the preparation of highly substituted carboxymethyl Cassia tora gum. Carbohydr Polym 157:527–532. https://doi.org/10.1016/j.carbpol.2016.10.049

Xia J, Yin S, Li H, Xu H, Xu L, Xu Y (2011) Improved visible light photocatalytic activity of sphere-like BiOBr hollow and porous structures synthesized via a reactable ionic liquid. Dalton Trans 40:5249–5258

Yu H et al (2017) Liquid-phase exfoliation into monolayered BiOBr nanosheets for photocatalytic oxidation and reduction. ACS Sustain Chem Eng 5:10499–10508. https://doi.org/10.1021/acssuschemeng.7b02508

Zhang XC, Zhao LJ, Fan CM, Liang ZH, Han PD (2012) First-principles investigation of impurity concentration influence on bonding behavior, electronic structure and visible light absorption for Mn-doped BiOCl photocatalyst. Phys B 407:4416–4424. https://doi.org/10.1016/j.physb.2012.08.002

Zhang B, Ji G, Gondal MA, Liu Y, Zhang X, Chang X, Li N (2013) Rapid adsorption properties of flower-like BiOI nanoplates synthesized via a simple EG-assisted solvothermal process. J Nanoparticle Res 15:1773. https://doi.org/10.1007/s11051-013-1773-4

Zhou P et al (2019a) Functionalization of cotton fabric with bismuth oxyiodide nanosheets: applications for photodegrading organic pollutants, UV shielding and self-cleaning. Cellulose 26:2873–2884. https://doi.org/10.1007/s10570-019-02281-8

Zhou P et al (2019b) Construction of a metallic silver nanoparticle-decorated bismuth oxybromide-based composite material as a readily recyclable photocatalyst. J Clean Prod. https://doi.org/10.1016/j.jclepro.2019.119007